

FIG. 2. (Color online) Drain characteristics of the Ta₂O₅/AlN/GaN HEMT (destructive breakdown occurs at 96 V for V_{GS}=-7 V).

Device processing was initiated by an Ohmic-first sequence. Ohmic contacts were formed by a shallow premetallization etch prior to the deposition of a Ti/Al/Ni/Au metal stack and an 800 °C anneal.¹⁴ This process yielded a contact resistance (R_c) of 0.7 Ω mm as measured by the transmission line method. A 6 nm ALD Ta₂O₅ layer was blanket deposited following a 100 nm deep, Cl-based, mesa isolation etch. Ta₂O₅ films were prepared using an ALD process utilizing pentakis(dimethylamino)tantalum (PDMAT) and water as reagents at 250 °C. The films were deposited in a hot wall flow tube type reactor.¹⁵ A constant flow of ultrahigh purity N₂ gas (15 sccm) was used to maintain a flow tube process-pressure of 200 mTorr during deposition and a 30 s purge time was used to separate the reagent pulses. Under these conditions linear growth was observed and a growth rate of 0.6 Å/cycle was measured using spectroscopic ellipsometry. As-deposited films were found to be amorphous and slightly overoxidized (O:Ta=3.0±0.3) with a bonded carbon content of ~5 at. %. Atomic force microscopy of the Ta₂O₅ film deposited on the AlN surface had a RMS roughness of 0.58 nm for the 1×1 μ m scan shown in Fig. 1 (RMS roughness of the as-grown AlN surface was 0.45 nm). Ta₂O₅ films received no postdeposition thermal treatments. Electron-beam lithographic definition of submicron gates with a T-profile concluded the device processing. Pertinent geometric dimensions of the HEMTs were source-drain separation (L_{SD}) of 3 μ m, gate width (W_g) of 2×25 μ m, and gate footprint length (L_g) of ~150 nm. On-wafer room-temperature Hall measurements were taken after the Ta₂O₅ deposition and sheet resistance was found to be 356 Ω/\square with a two-dimensional electron density and mobility of 2.2×10^{13} cm⁻² and 800 cm²/Vs, respectively.

Drain characteristics are shown in Fig. 2 with a maximum current density of 1.37 A/mm at V_{GS}=4 V. Corresponding transfer characteristics were taken at V_{DS}=8 V and shown in Fig. 3(a). A maximum extrinsic transconductance (g_m) was measured to be 315 mS/mm. Taking into account source contact (0.7 Ω mm) and access (0.21 Ω mm) resistance, this value corresponds to an intrinsic $g_m^{\text{int}} \sim 450$ mS/mm. Gate current was found to be the limiting in off-state drain current [Fig. 3(b)]. Low (10^{-8} A/mm) parallel conduction in the buffer layer was measured.

Off-state breakdown voltage is often defined by the criterion that 1 mA/mm drain current density is reached in the

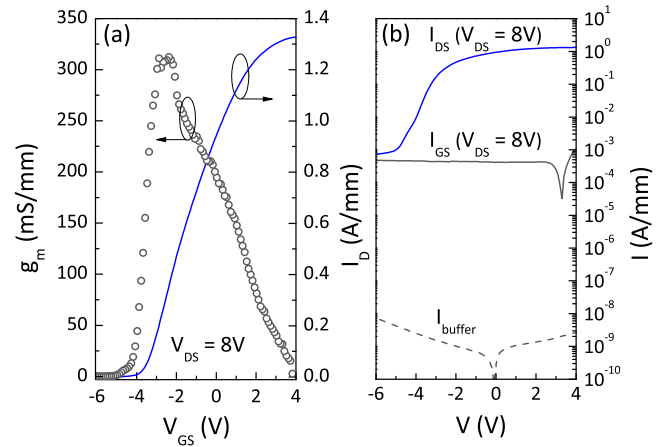


FIG. 3. (Color online) Transfer (a) and gate current (b) characteristics of the Ta₂O₅/AlN/GaN HEMT.

subthreshold state. According to this metric, $V_{BD} \sim 30$ V. However, the Ta₂O₅-insulated devices ultimately sustained drain-source voltages of up to 96 V under off-state gate-source bias (V_{GS}=-7 V) before destructively breaking down (Fig. 2) demonstrating an $\sim 5\times$ increase of this particular characteristic over other reports.²⁻⁷ It is noted that after ~ 60 V drain voltage sweep in off-state conditions, the device's low-voltage I_{DS} and g_m degraded by 30–50 %. The pre-DBD degradation is speculated to be the result of a localized breakdown of the AlN barrier at the drain edge of the gate under reverse bias forcing the Ta₂O₅ to sustain the entire voltage drop. This would still maintain transistor action after AlN breakdown but with degraded transport across the gated region. It is therefore plausible that DBD occurs after AlN breakdown when the local electric field is of sufficient intensity to cause electrical failure of the Ta₂O₅ film.

Terman's high-frequency C-V method¹⁶ has been adapted for the stacked oxide/barrier structure in order to investigate the Ta₂O₅/AlN interface. The C-V functionality of the Ta₂O₅/AlN/GaN structure may be acquired through Poisson's equation and is found to yield the total "ideal" capacitance: $C_{\text{tot}} = (1/C_{\text{ox}} + 1/C_{\text{AlN}} + 1/C_Q)^{-1}$. C_{ox} and C_{AlN} are the fixed oxide and AlN barrier capacitances and $C_Q = qN_{\text{eff}}/kT(1 + e^{-\eta_s})^{-1}$ is the quantum capacitance of the GaN well (QW) assuming population of only one subband, E_o . $N_{\text{eff}} = m^*kT/\pi\hbar^2$ is the effective conduction band density of states and $\eta_s = (E_F - E_o)/kT$ is the normalized local potential at the GaN QW (see Fig. 1). The assumption of single subband population may lead to some error for conditions that cause high 2DEG population. The Fermi level in the channel is affected by the occupation of interface states which causes C-V stretch-out. The charge-field relationship between the two charge distributions may be found by considering a voltage loop starting from the oxide/AlN interface and terminating at the Fermi level in the GaN QW

$$kT\eta_i - qV_{\text{AlN}} - \Delta E_C + E_o + kT\eta_s = 0, \quad (1)$$

where $kT\eta_i = E_{C,i} - E_F$ is the local potential at the oxide/AlN interface, $V_{\text{AlN}} = q(\sigma_{\text{net}}^{\pi} - n_s)/C_{\text{AlN}}$ is the voltage drop in the AlN barrier, and ΔE_C is the AlN/GaN conduction band discontinuity. Interface trap state density, D_{it} , may be found by $qkTD_{it} = \partial Q_{it}/\partial \eta_i$ and applying Terman's method which compares the difference between the ideal and trapped charge laden systems

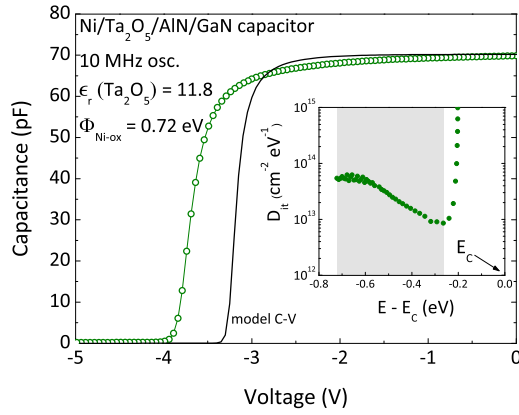


FIG. 4. (Color online) Measured (circle) and modeled (line) C-V characteristic of the Ta₂O₅/AlN/GaN capacitor. Inset shows D_{it} spectrum.

$$D_{it} = \frac{C_{ox}}{qkT} \frac{\partial \Delta V_{GS}}{\partial \eta_i}, \quad (2)$$

where $\Delta V_{GS} = V_{GS,meas} - V_{GS,ideal}$ at common capacitance.

Figure 4 shows C-V characteristics measured at room-temperature alongside the modeled ideal C-V curve for the voltage comparison. The resultant interfacial density spectrum is shown in the inset. The metal-insulator energy barrier and band-offset to AlN were taken as 0.72 and -2.5 eV, respectively, based off Robertson's work.¹¹ Inaccuracies in these values will lead to error in the energetic location of the traps but does not interfere with the calculation of D_{it} . The abrupt increase in D_{it} near band edge may be due in part to an increased band edge state density owing to the termination of the crystal periodicity at the surface.¹⁷ D_{it} was found to range between $0.9-6 \times 10^{13}$ cm⁻² eV⁻¹ (gray region).

Terman's method implicitly probes interfacial charge states which are below the ac perturbation frequency thus, fast states are not accounted for. These "slow" states apparently do not impose deleterious effects on small signal frequency performance as can be seen in Fig. 5. Small-signal S-parameter characteristics were taken at the bias point that yielded maximum g_m . Extrinsic values of unity current gain frequency (f_t) and maximum frequency of operation (f_{max}) were measured to be 55 and 115 GHz, respectively. By employing the ColdFET and standard Y-subtraction technique,¹⁸ pad parasitics were modeled (table inset, Fig. 5) and the de-embedded value of f_t was determined to be 75 GHz.

AlN/GaN HEMTs employing a 6 nm thick ALD Ta₂O₅ film for gate current suppression have been reported. The gate oxide enabled V_{DS} biases up to 96 V before destructive breakdown. Maximum current density of 1.37 A/mm and extrinsic transconductance of 315 mS/mm was measured. Respective small signal frequency performance of and 115 GHz for f_t and f_{max} , was obtained despite a relatively high D_{it} . With further optimization of heterostructure growth, shorter gate lengths, and the usage of Ta₂O₅ thin films for gate insulation and improved robustness, the efficacy of the

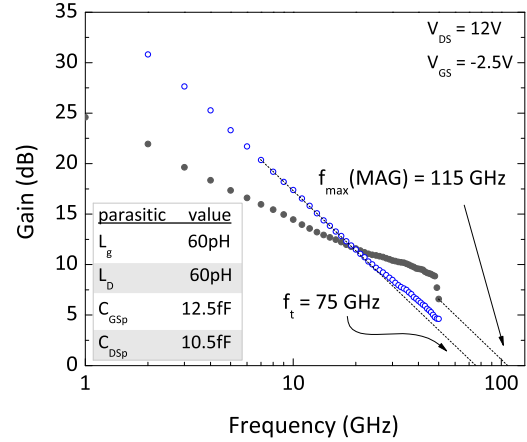


FIG. 5. (Color online) Small-signal frequency performance of the Ta₂O₅/AlN/GaN HEMT.

AlN/GaN HEMT to push the boundary of frequency-power operation of III-V semiconductor technology may be attained.

The authors acknowledge N. Green for his assistance with processing. D. A. Deen thanks J. G. Champlain and M. G. Ancona for technical discussions. This work was supported by the Office of Naval Research. The Ta₂O₅ ALD work at UMBC was supported in part by NSF (Grant No. DMR 0846445).

¹Y. Cao and D. Jena, *Appl. Phys. Lett.* **90**, 182112 (2007).

²A. M. Dabiran, A. M. Wowchak, A. Osinsky, J. Xie, B. Hertog, B. Cui, D. C. Look, and P. P. Chow, *Appl. Phys. Lett.* **93**, 082111 (2008).

³T. Zimmermann, D. Deen, Y. Cao, J. Simon, P. Fay, D. Jena, and H. Xing, *IEEE Electron Device Lett.* **29**, 661 (2008).

⁴M. Higashiwaki, T. Mimura, and T. Matsui, *IEEE Electron Device Lett.* **27**, 719 (2006).

⁵N. Onojima, N. Hirose, T. Mimura, and T. Matsui, *Appl. Phys. Lett.* **93**, 223501 (2008).

⁶D. Deen, T. Zimmermann, Y. Cao, D. Jena, and H. G. Xing, *Phys. Status Solidi C* **5**, 6 (2008).

⁷D. A. Deen, S. C. Binari, D. F. Storm, D. S. Katzer, J. A. Roussos, J. C. Hackley, and T. Gougousi, *Electron. Lett.* **8**, 45 (2009).

⁸S. Seo, G. Y. Zhao, and D. Pavlidis, *Electron. Lett.* **44**, 3 (2008).

⁹H. Xing, Y. Dora, A. Chini, S. Heikman, S. Keller, and U. Mishra, *IEEE Electron Device Lett.* **25**, 161 (2004).

¹⁰L. W. Tu, W. C. Kuo, K. H. Lee, P. H. Tsao, C. M. Lai, A. K. Chu, and J. K. Sheu, *Appl. Phys. Lett.* **77**, 3788 (2000).

¹¹J. Robertson and B. Falabretti, *J. Appl. Phys.* **100**, 014111 (2006).

¹²D. F. Storm, D. S. Katzer, S. C. Binari, B. V. Shanabrook, L. Zhou, and D. J. Smith, *Appl. Phys. Lett.* **85**, 3786 (2004).

¹³O. Brandt, R. Muralidharan, P. Waltereit, A. Thamm, A. Trampert, H. von Kiedrowski, and K. H. Ploog, *Appl. Phys. Lett.* **75**, 4019 (1999).

¹⁴D. A. Deen, D. F. Storm, D. S. Katzer, D. J. Meyer, and S. C. Binari, *Solid-State Electron.* **54**, 613 (2010).

¹⁵J. C. Hackley, J. D. Demaree, and T. Gougousi, *J. Appl. Phys.* **102**, 034101 (2007).

¹⁶L. M. Terman, *Solid-State Electron.* **5**, 285 (1962).

¹⁷C. Kittel, *Introduction to Solid State Physics*, 8th ed. (Wiley, Hoboken, 2005), Chap. 17.

¹⁸G. Dambrine, A. Cappy, F. Heliodore, and E. Playez, *IEEE Trans. Microwave Theory Tech.* **36**, 1151 (1988).